Molecular Cell
Short Article

# tRNA Binding, Structure, and Localization of the Human Interferon-Induced Protein IFIT5

George E. Katibah,[1] Ho Jun Lee,[1,3] John P. Huizar,[1,3] Jacob M. Vogan,[1] Tom Alber,[1,2] and Kathleen Collins[1,2,*]
[1]Department of Molecular and Cell Biology
[2]California Institute of Quantitative Biosciences (QB3)
University of California, Berkeley, Berkeley, CA 94720, USA
[3]These authors contributed equally to this work
*Correspondence: kcollins@berkeley.edu
http://dx.doi.org/10.1016/j.molcel.2012.12.015

## SUMMARY

**Interferon-induced proteins, including the largely uncharacterized interferon-induced tetratricopeptide repeat (IFIT) protein family, provide defenses against pathogens. Differing from expectations for tetratricopeptide repeat (TPR) proteins and from human IFIT1, IFIT2, and IFIT3, we show that human IFIT5 recognizes cellular RNA instead of protein partners. In vivo and in vitro, IFIT5 bound to endogenous 5′-phosphate-capped RNAs, including transfer RNAs. The crystal structure of IFIT5 revealed a convoluted intramolecular packing of eight TPRs as a fold that we name the TPR eddy. Additional, non-TPR structural elements contribute to an RNA binding cleft. Instead of general cytoplasmic distribution, IFIT5 concentrated in actin-rich protrusions from the apical cell surface colocalized with the RNA-binding retinoic acid-inducible gene-I (RIG-I). These findings establish compartmentalized cellular RNA binding activity as a mechanism for IFIT5 function and reveal the TPR eddy as a scaffold for RNA recognition.**

## INTRODUCTION

Viral infection triggers a broad host response that cripples metabolism and limits viral replication. Secreted cytokines such as the type I interferons (IFNs) are potent inducers of innate immune response gene expression programs for antiviral defense (Schoggins and Rice, 2011; Diamond and Farzan, 2013). Among the most strongly type I IFN-induced gene products are several proteins predicted to contain multiple tetratricopeptide repeats (TPRs) (Schoggins and Rice, 2011; Fensterl and Sen, 2011). These interferon-induced tetratricopeptide repeat (IFIT) proteins are believed to restrict viral infections by binding in an inhibitory manner to virus-specific targets, as well as to host-cell eIF3, a protein complex essential for translation initiation (Fensterl and Sen, 2011; Sen and Fensterl, 2012; Diamond and Farzan, 2013). Human IFIT1, IFIT2, and IFIT3 appear to have concerted functions as interacting homodimers, heterodimers, and/or oligomers (Stawowczyk et al., 2011; Pichlmair et al., 2011; Fensterl and Sen, 2011; Yang et al., 2012). Humans have a fourth IFIT family member, IFIT5, which, unlike IFIT1, IFIT2, and IFIT3, has no murine ortholog (Schoggins and Rice, 2011; Fensterl and Sen, 2011). Curiously, IFIT5 is excluded from association with IFIT1, IFIT2, and IFIT3 and also lacks any other strongly interacting protein partner (Hogg and Collins, 2007a; Pichlmair et al., 2011).

In other multi-TPR proteins, the bihelical repeats pack regularly to create an extended superhelical platform for protein-protein interactions (D'Andrea and Regan, 2003; Zhu et al., 2012; Zeytuni and Zarivach, 2012). The precedent of TPR-scaffolded assembly of protein complexes fits with the observed multimerization of human IFIT1, IFIT2, and IFIT3 and their nucleation of a much larger IFIT1/IFIT2/IFIT3 protein interactome (Pichlmair et al., 2011). Here we show that IFIT5 does not fit this paradigm for TPR protein function. We demonstrate that a monomer of IFIT5 binds directly, specifically, and autonomously to endogenous human cell RNAs with 5′ phosphate ends, including transfer RNAs (tRNAs). RNA recognition requires a convoluted intramolecular fold of the IFIT5 TPRs, which scaffolds unique additional helices that form an RNA binding cleft. Remarkably, IFIT5 and the antiviral double-stranded RNA-binding protein retinoic acid-inducible gene-I (RIG-I) colocalize in actin-rich structures at the apical cell surface, suggesting a general significance for cell-peripheral compartmentalization of innate immune response proteins with RNA ligands.

## RESULTS AND DISCUSSION

To gain insight about IFIT5 function, we characterized its cellular binding partners. We expressed triple-FLAG-tagged (3xF) human IFIT5 with (Figures 1A–1C) or without (Figures S1A–S1C available online) IFN-β treatment of transiently transfected HEK293T cells. No consistent IFIT5 copurification of other proteins was detected (Figure S2). In contrast, denaturing gel electrophoresis and SYBR Gold staining of RNA in the input versus IFIT5-bound samples showed selective IFIT5 enrichment of RNAs that were approximately the size of tRNAs but distinct from the tRNA pool of the input cell extract (Figures 1B and S1B). Similar RNA coenrichment was observed upon purification of IFIT5 from HeLa cells (Figures S1D–S1F). Compared to IFIT5, human IFIT1, IFIT2, and IFIT3, as well as the mouse IFIT2 proposed to functionally parallel human IFIT5 (Daffis et al., 2010), did not copurify a similar amount or profile of cellular

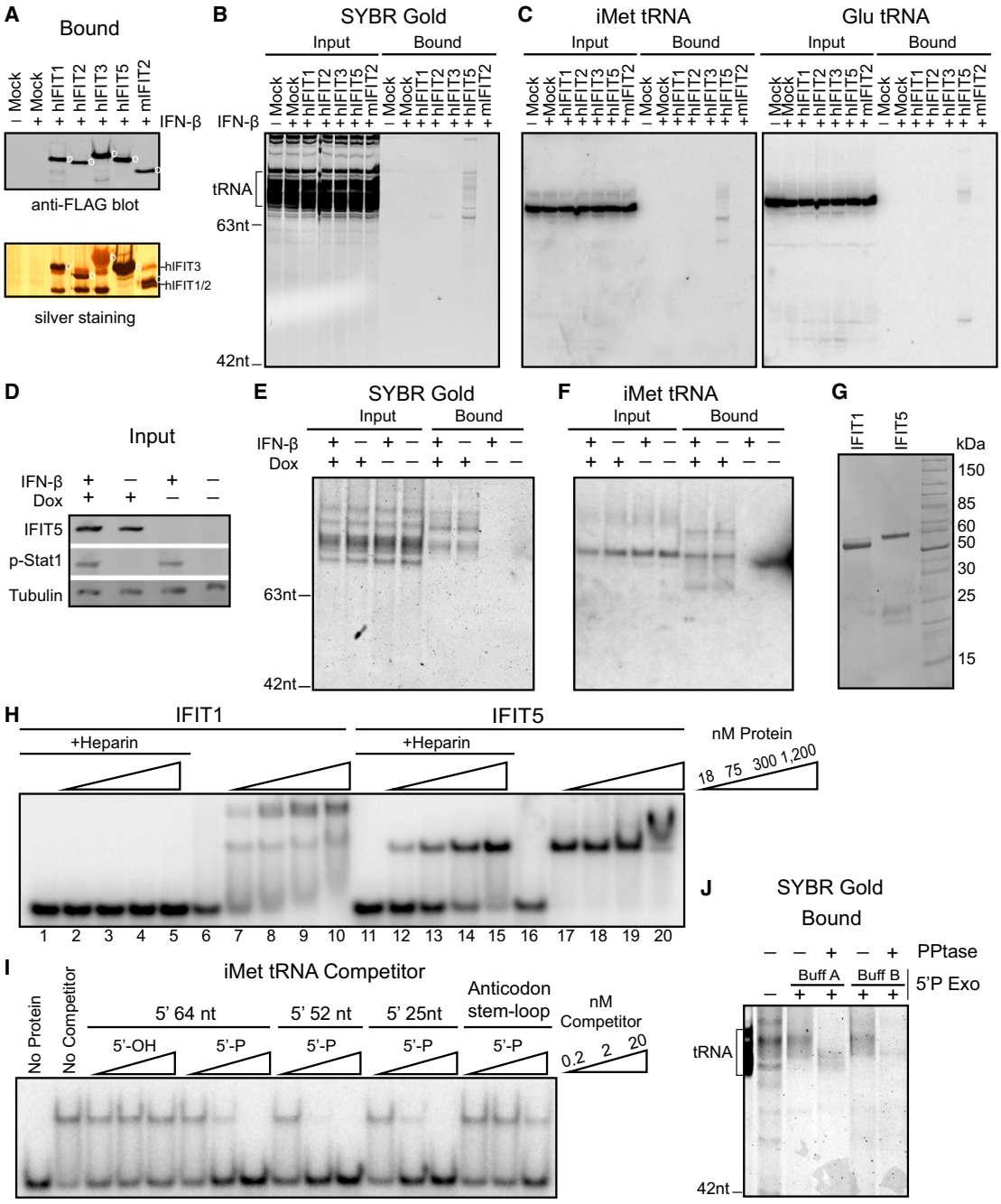


**Figure 1. IFIT5 RNA Binding Specificity**

(A–C) HEK293T cells were transfected to express a human IFIT protein or mouse IFIT2 with an N-terminal 3xF tag. Mock indicates no tagged protein expression. Cells were treated with IFN-β as indicated. Protein purification was detected by anti-FLAG immunoblot (A, upper panel) or silver staining (A, lower panel) with the tagged protein in each lane indicated by an open circle; note that IFIT3 stained light orange. Copurified RNA was detected by SYBR Gold (B), and blot hybridization of the gel in (B) was used to detect the 5′ end of specific tRNAs (C).

(D–F) HEK293 cells expressing a doxycycline (Dox)-inducible 3xF-IFIT5 transgene were used for denaturing affinity purification after in vivo crosslinking. Y701-phosphorylated Stat1 established IFN response induction, and tubulin was a normalization control (D). Coenriched RNAs were detected by staining (E) or blot hybridization (F).

(G–I) Recombinant IFIT1 and IFIT5 were detected by Coomassie blue R-250 staining (G) and used for EMSA with in vitro-transcribed and radiolabeled 64 nt iMet tRNA (H), with unlabeled competitor RNAs mixed with IFIT5 prior to addition of the radiolabeled 64 nt iMet tRNA (I).

(J) RNA bound to HEK293 transgene-expressed 3xF-IFIT5 from nondenaturing cell extract was used for parallel treatments with 5′ polyphosphatase (PPtase) and/or Terminator exonuclease (5′P Exo) in Terminator buffer A or B prior to gel resolution and SYBR Gold staining.

See also Figures S1–S4.

RNA (Figures 1B and S1B), whether assembled with other IFIT proteins in cells treated with IFN-β (Figure 1A, lower panel) or purified alone (Figure S1A, lower panel).

To establish whether the tRNA-sized RNAs that copurified with IFIT5 actually included tRNAs, we used northern blot hybridization. Northern blots revealed the presence of IFIT5-bound initiator methionine (iMet) tRNA and, to a lesser extent, some of the additional tRNAs tested (Figures 1C, S1C, and S1F). Curiously, a probe complementary to the iMet tRNA 5′ end detected numerous sizes of coenriched RNA, including a prominent fragment ~10 nt shorter than full-length mature tRNA that was not detected with a probe for the iMet tRNA 3′ end (Figures S1C and S1F). Other tRNA 5′ end probes also detected forms of IFIT5-bound tRNA different in size from mature tRNA (Figures 1C, S1C, and S1F). The extent of iMet tRNA 3′ truncation was investigated by ligation of IFIT5-enriched RNA to an adaptor oligonucleotide, reverse transcription, and PCR with an iMet tRNA forward primer. Cloned sequences included 3′-truncated iMet tRNA with a mismatch to genomic sequence anticipated by tRNA base modification and an appended 3′ polyuridine tract (Figure S3). Polyuridine tailing has been previously reported for RNA degradation intermediates (Norbury, 2010). Truncation and/or tailing of IFIT5-bound tRNAs would give rise to tRNA sizes different from mature tRNA.

Paralleling a previous strategy to mimic an endogenously induced level of IFIT protein expression (Pichlmair et al., 2011), we expressed IFIT5 from a doxycycline-regulated transgene stably integrated in HEK293 cells. Also, to eliminate any reassortment of complexes after cell lysis, we purified the transgene-expressed IFIT5 under stringently denaturing conditions after in vivo crosslinking with formaldehyde (Niranjanakumari et al., 2002). IFIT5 specifically copurified crosslinked tRNA-sized RNAs, including iMet tRNA of precisely the mature tRNA size (Figures 1D–1F). The profile of IFIT5-bound RNA was not affected by treatment of cells with IFN-β (Figures 1D–1F). Because IFIT5 consistently copurified forms of iMet tRNA longer and shorter than the mature tRNA that were not abundant in the input cell extract, and considering the substantial in vivo accumulation of ~30 and ~45 nt RNA fragments induced by high IFIT5 overexpression (Figure S1B), we speculate that IFIT5-bound tRNAs are preferentially targeted for degradation. The tRNA fragments copurified with IFIT5 could represent intermediates in tRNA degradation that were stabilized by IFIT5 binding, tRNA secondary structure, and/or tRNA base modification.

To test for direct binding of iMet tRNA by IFIT5, we reconstituted the protein-RNA interaction using bacterially expressed and purified IFIT5 (Figure 1G) and in vitro transcribed iMet tRNA lacking the 3′ ~10 nt not required for robust IFIT5 copurification of iMet tRNA from cell extract (Figures 1C, 1F and S1C, S1F, and S3). The 5′ monophosphate present on mature tRNAs in vivo was conferred by radiolabeling of a precisely defined RNA sequence excised from a longer in vitro transcript (Fechter et al., 1998). By native electrophoretic gel mobility shift assay (EMSA), IFIT5 bound to iMet tRNA in the absence or presence of heparin, a standard competitor of nonspecific RNA interactions (Ryder et al., 2008). Notably, IFIT5 produced a single RNA mobility shift at all but the highest, micromolar concentration of recombinant protein (Figure 1H, lanes 11–20). In comparison, the human IFIT1 reported to bind 5′-triphosphate-capped RNAs (Pichlmair et al., 2011) did not bind the 5′-monophosphate-capped iMet tRNA in the presence of heparin (Figure 1H, lanes 1–5). Without heparin, IFIT1 gave heterogeneous mobility shifts requiring higher protein concentration than RNA binding by IFIT5 (Figure 1H, lanes 6–10).

Bacterially expressed IFIT5 bound iMet tRNA dependent on the 5′ monophosphate (Figure 1I). IFIT5 preferentially bound 3′-truncated tRNA, but the full-length iMet tRNA and other full-length tRNAs could compete for IFIT5 binding as long as they contained a 5′ monophosphate (Figure S4A). A series of iMet tRNA 5′ fragments with successively larger 3′ truncations retained competition for IFIT5 binding, but the isolated anticodon stem loop did not (Figure 1I). Direct binding assays confirmed that IFIT5 preferentially bound the iMet tRNA fragments with a truncated 3′ end compared to the full-length tRNA or anticodon stem loop, both of which would be predicted to have a base-paired rather than single-stranded 5′ end (Figure S4B). In vitro transcribed RNAs with a 5′ triphosphate were not more effective competitors for IFIT5 binding than a 5′ monophosphate RNA, yet both were strong competitors relative to the corresponding RNA without any 5′ phosphate group (Figure S4C). Purified IFIT5-bound cellular RNAs were assayed for degradation by a 5′-monophosphate-dependent exonuclease, with or without pretreatment by a polyphosphatase to convert any 5′ polyphosphate ends to 5′ monophosphate. Much of the bound cellular RNA was degraded even without polyphosphatase treatment, consistent with the presence of a 5′ monophosphate, and almost all of the remaining RNA was degraded after 5′ polyphosphate conversion to 5′ monophosphate (Figure 1J). Together these results demonstrate IFIT5 binding to endogenous cellular RNAs with at least one 5′ phosphate group. Mature tRNAs are an abundant pool of monophosphate-capped cellular RNAs that, in their cycle between aminoacyl synthetase and ribosome interactions, would be highly accessible for IFIT5 binding. Because the mature iMet tRNA forms a relatively weak A-U base pair at its 5′ end required for eukaryotic initiator tRNA function (Farruggio et al., 1996), it may be particularly prone to acceptor stem fraying and IFIT5 association in vivo.

To define the structural basis for IFIT5 RNA recognition, we determined the crystal structure of IFIT5 at 2.2 Å resolution (Table 1 and Figure S5). The IFIT5 secondary structure is composed entirely of helices, including eight TPRs (Figure 2A). Consistent with the IFIT5 monomer evident by gel filtration (Figure S6), the TPRs pack with exclusively intramolecular contacts to form a fold that we term the TPR eddy (Figure 2A). The N-terminal 46 amino acids of IFIT5 constitute an extended buttress framing the first three TPRs, which at first reach toward the protein N terminus (TPR1 and TPR2) and then double back (TPR 3). A two-helix insertion positions the subsequent TPR4 and TPR5, followed by an abrupt turn introduced by another helical hairpin (residues 283–333) that projects an arm between TPR5 and TPR6. Reminiscent of the tRNA recognition arm of seryl-tRNA synthetase (Cusack et al., 1996), the arm of IFIT5 contributes one side of a deep cleft lined with basic side chains (Figures 2A and 2B) that is completed by packing of TPR6 and TPR7 and a non-TPR connecting helix (residues 413–427). TPR 8 and a C-terminal helix (residues 469–478) cap the end of the

**Table 1. Crystallographic Data Collection and Refinement Statistics**

| | Native | SeMet: Peak | SeMet: Remote |
|---|---|---|---|
| Data Collection | | | |
| Space group | $P2_12_12_1$ | $P2_12_12_1$ | |
| Cell dimensions: *a*, *b*, *c* (Å) | 63.83, 71.79, 116.92 | 64.07, 71.73, 116.45 | |
| Cell dimensions: α, β, γ (°) | 90, 90, 90 | 90, 90, 90 | 90, 90, 90 |
| Wavelength | 1.1111 | 0.97965 | 0.96817 |
| Resolution (Å) | 50–2.2 (2.24–2.20) | 50–2.85 (2.90–2.85) | 50–2.85 (2.90–2.85) |
| $R_{sym}$ or $R_{merge}$ | 0.114 (0.699) | 0.137 (0.616) | 0.135 (0.627) |
| $I / \sigma I$ | 14.6 (2.0) | 20.8 (4.3) | 20.6 (4.3) |
| Completeness (%) | 99.9 (100) | 100 (100) | 100 (100) |
| Redundancy | 4.0 (4.0) | 8.2 (8.4) | 8.2 (8.5) |
| Refinement | | | |
| Resolution (Å) | 47.70–2.20 | | |
| No. reflections | 27,860 | | |
| $R_{work}$ / $R_{free}$ | 0.1778 / 0.2398 | | |
| Number of atoms: Protein | 3,913 | | |
| Number of atoms: Ligand/ion | 7 | | |
| Number of atoms: Water | 232 | | |
| *B* factors: Protein | 26.66 | | |
| *B* factors: Ligand/ion | 46.84 | | |
| *B* factors: Water | 28.87 | | |
| Rmsd: Bond lengths (Å) | 0.008 | | |
| Rmsd: Bond angles (°) | 1.121 | | |
| Ramachandran statistics: Most-favored regions | 98.3% | | |
| Ramachandran statistics: Allowed regions | 1.7% | | |
| Ramachandran statistics: Disallowed regions | 0.0% | | |

Values in parentheses are for the highest-resolution shell.

TPR eddy (Figure S7), creating a prominent saddle between the N- and C-terminal lobes of the protein (Figures 2A and 2B).

The contorted TPR eddy of IFIT5 differs from the extended superhelical arrangement of TPRs in other multi-TPR proteins (D'Andrea and Regan, 2003; Zeytuni and Zarivach, 2012). The IFIT5 TPR eddy has overall similarity but local and global differences with the recently reported structure of a human IFIT2/ISG54 dimer (Yang et al., 2012). IFIT2 dimerization occurs by domain swapping of a three-helix bundle containing TPR3, as well as other cross-subunit appositions enabled by a hinged closing of the cleft and opening of the saddle (Figures 2C and S8). The IFIT5 cleft has sequence conservation across IFIT5 proteins (Figure 2D) and unique to IFIT5 proteins (Figure S9) that can underlie structural differences between IFIT5 and IFIT2 (Figure S8), IFIT5 exclusion from the homo- and heterodimerizations observed for IFIT1, IFIT2, and IFIT3 (Sen and Fensterl, 2012), and the unique IFIT5 RNA binding specificity (Figures 1B and S1B). However, mapping the IFIT5 structural elements (Figure 2A) on to a primary sequence alignment of human IFIT family members (Figure S9) suggests that all IFIT family members could form a TPR eddy.

We investigated IFIT5 structural requirements for RNA binding using C-terminal truncations from the beginning of TPR7 or TPR8 (Figure 3A). IFIT5 copurification of cellular RNAs, including iMet tRNA, was reduced by C-terminal truncation from TPR8 (TPRΔ8) and eliminated by truncation from TPR7 (TPRΔ7−8) (Figures 3B and 3C). Likewise, the bacterially expressed and purified TPRΔ8 showed partially reduced iMet tRNA binding activity, and TPRΔ7−8 retained no RNA binding activity (Figures 3D and 3E). The truncation from TPR7 would eliminate one side of the cleft (Figure 2A). As expected for an RNA binding site, the cleft has the greatest positive surface potential in the structure (Figure 2B), and side chains project into the cleft with conformational flexibility (Figure S5).

We substituted individual residues in the cleft with alanine (Figure 3F), targeting solvent-accessible side chains with sequence conservation among IFIT5 orthologs (Figure S9). IFIT5 variants with a L291A, K302A, R307A, K309A, F388A/H389A, K415A, K422A, or K426A substitution were expressed to comparable levels in HEK293T cells and purified comparably (Figure 3G). All of the cleft side-chain substitutions except L291A, which was deepest in the cleft (Figure 3F), reduced IFIT5 cellular RNA binding activity (Figure 3H). We compared the direct iMet tRNA binding activity of bacterially expressed, purified proteins across a range of in vivo RNA binding deficiency using the L291A, R307A, K415A, and K426A sequence variants (Figure 3I). Paralleling the results of cellular IFIT5 expression, the purified IFIT5 proteins demonstrated an in vitro iMet tRNA binding activity that was near normal for the L291A protein, 5-fold reduced for the K426A protein, or more than 25-fold reduced for the R307A and K415A proteins (Figure 3J). These results strongly implicate the IFIT5 arm and cleft as an RNA binding site.

To understand the cellular context for IFIT5 RNA binding, we investigated the localization of IFIT5 expressed by transient transfection (Figure 4) or by inducible expression from the integrated transgene (Figure S10). Both 3xF-IFIT5 (Figures 4A and S10) and IFIT5 tagged with mCherry (Figure 4B) localized to actin-rich protrusions of the apical cell surface. Similar microvillus-like projections are present in many cell types (Chhabra and Higgs, 2007; Lange, 2011), and, correspondingly, these projections were present independent of IFIT5 expression (Figure 4A, compare the cell at upper left versus the lower right). IFIT5 subcellular localization was not overtly altered by treatment of cells with IFN-β (Figure S10). IFIT5 localization appeared to be at least partially independent of RNA binding, because at least some of the C-terminally truncated, RNA-binding defective TPRΔ7−8 protein colocalized with actin (Figure 4A, lower panels). In fibroblast-derived cells with well-resolved actin

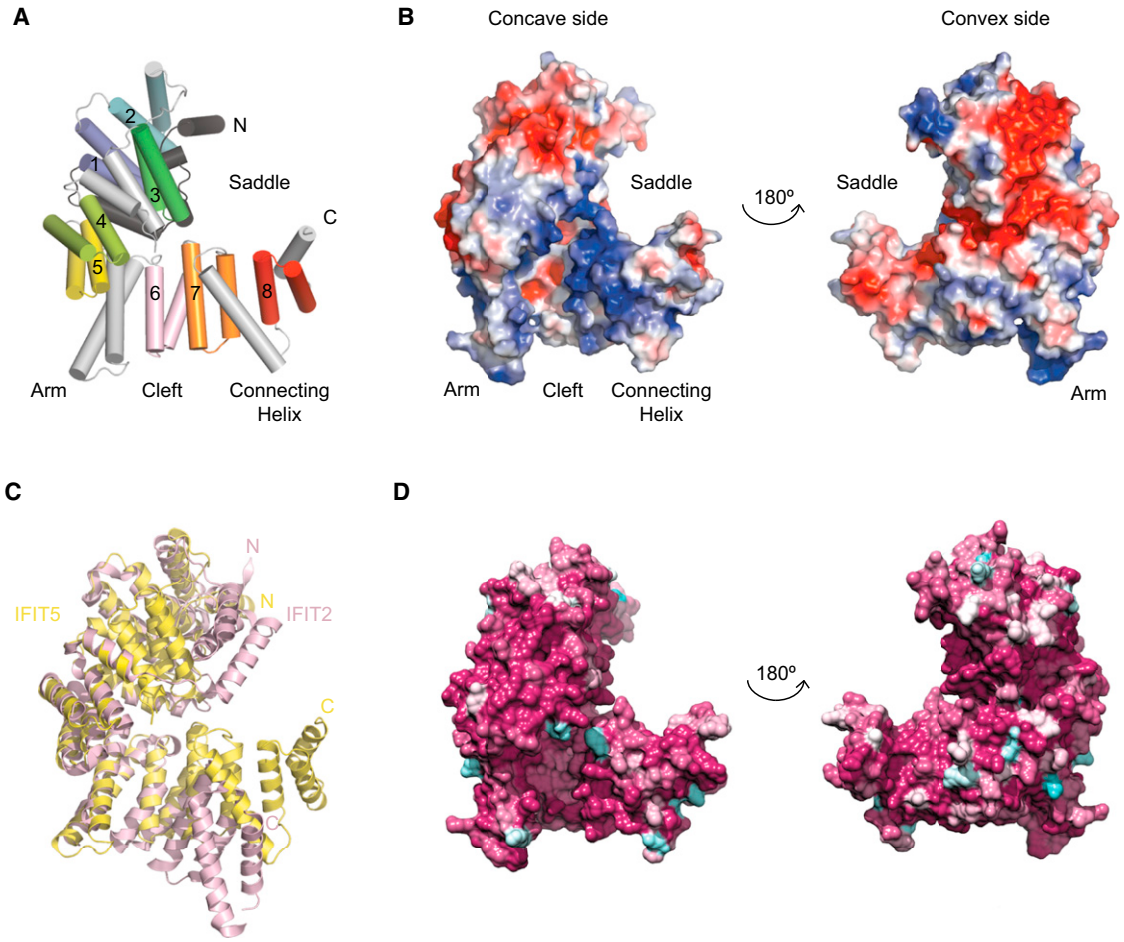


**Figure 2. The TPR Eddy of IFIT5**

(A) The structure of IFIT5 is depicted with cylinders representing helices. TPRs (separately colored, and the first helix of each numbered) are interspersed with non-TPR elements (gray). N and C termini are indicated.

(B) Electrostatic potential surface representation of IFIT5. Views are related by 180° rotation, with the view on the left similar to that in (A). Blue and red contours begin at +3 and −3 kT, respectively.

(C) Ribbon diagram of IFIT5 (yellow) superimposed on a monomer from the domain-swapped IFIT2 dimer (pink). N and C termini are indicated.

(D) Sequence conservation among IFIT5 proteins plotted from magenta (conserved) to cyan (variable) on the protein surface, based on primary sequence alignment (Figure S9). Views are related by 180° rotation, with the view on the left similar to that in (A).

See also Figures S5–S9.

structures (Figure 4A), IFIT5 concentrated specifically in the microvillus-like structures at the apical cell surface. In hepatocyte-derived Huh7 cells (Figure 4B), IFIT5 also colocalized with the apical cell surface membrane ruffles that move rearward from a cell's leading edge and coalesce to form macroscopic actin filament rings (Chhabra and Higgs, 2007).

The antiviral sensor RIG-I, which recognizes double-stranded 5′-triphosphate-capped RNA (Kolakofsky et al., 2012; Berke et al., 2012), has also been detected in actin-containing projections from the cell surface (Mukherjee et al., 2009). We found that mCherry-tagged IFIT5 and green fluorescent protein (eGFP)-tagged RIG-I concentrated in the same apical cell surface microvillus-like and membrane ruffle structures (Figure 4B). Consistent with the observed localization of IFIT5 or RIG-I to actin structures without co-overexpression of the other protein, we did not detect a biochemical association of IFIT5 and RIG-I that was stable to purification from cell extract. We speculate that each protein independently adopts the same subcellular compartmentalization as a mechanism for influencing RNA ligand recognition and/or degradation, for example to limit RNA binding or degradation to the cell periphery or to link these activities to actin depolymerization at sites of pathogen contact and entry (Delorme-Axford and Coyne, 2011).

IFIT proteins other than IFIT5 have been reported to homo- and/or heterodimerize and to interact with diverse additional proteins as mechanisms of biological function (Fensterl and Sen, 2011; Sen and Fensterl, 2012; Diamond and Farzan, 2013). In addition, IFIT1 has binding activity for synthetic 5′-triphosphate-capped RNA and a recombinant IFIT2 homodimer has binding activity for synthetic AU-rich duplex RNA (Pichlmair

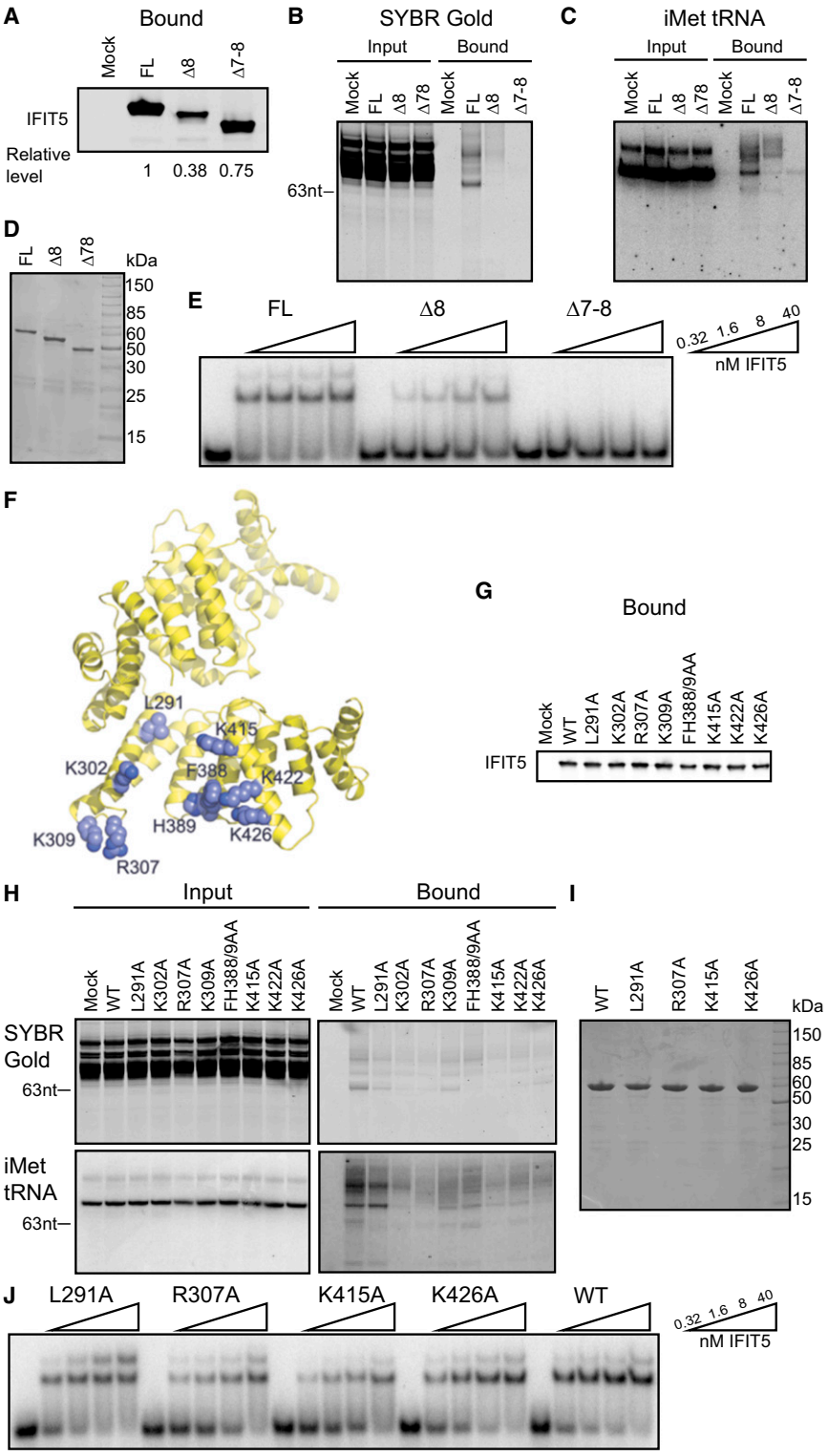


**Figure 3. An IFIT5 RNA Binding Cleft**

(A–C) C-terminally truncated proteins were expressed by transfection of HEK293T cells, with relative purified protein amounts determined by immunoblot (A), copurification of RNA visualized by SYBR Gold (B), and copurification of iMet tRNA tested by Northern blot (C).

(D–E) C-terminally truncated proteins purified from *E. coli* were detected by Coomassie blue R-250 staining (D) and used for EMSA with the 64 nt iMet tRNA (E).

(F) Space-filling representation of IFIT5 side chains individually targeted for mutational analysis, highlighted on the ribbon diagram of IFIT5.

(G and H) IFIT5 sequence variants were purified from transiently transfected HEK293T cells and detected by immunoblot (G), with input (left) and copurified (right) RNAs stained by SYBR Gold (top) and used for blot hybridization (bottom) to detect iMet tRNA (H).

(I and J) IFIT5 sequence variants purified from *E. coli* were detected by Coomassie blue R-250 staining (I) and used for EMSA with the 64 nt iMet tRNA (J).

See also Figure S9.

et al., 2011; Yang et al., 2012). It remains to be established how any RNA associations of IFIT1/IFIT2/IFIT3 complexes relate to their protein ligand interactions. Unlike the other human IFIT proteins, IFIT5 folds autonomously as a monomer without any apparent homo- or heterodimerization. The IFIT5 monomer harbors a deep cleft with positive surface potential that was not formed by an IFIT2 homodimer (Yang et al., 2012). Also unlike the other human IFIT proteins, IFIT5 readily recognizes cellular rather than only viral-hallmark RNA structures, accounting for the robust IFIT5 copurification of endogenous human RNAs from uninfected cells. We conclude that while IFIT5 retains the IFN-induced expression of other human IFIT family members, IFIT5 has evolved independent biochemical function and thus distinct antiviral activity (Schoggins et al., 2011).

Our determinations of IFIT5 structure and specific residues required for RNA binding provide knowledge about a previously unrecognized structural framework for protein-RNA interaction. With consistent in vivo and in vitro specificity, we find that IFIT5 binds tRNAs with a 5′ monophosphate group. This insight expands the scope of cellular tRNA fates, adding to the growing awareness of a new biology of tRNA roles, interaction partners, regulated modifications, processing reactions, and turnover pathways (Phizicky and Hopper, 2010; Sobala and Hutvagner, 2011; Geslain and Pan, 2011; Hasler and Meister, 2012). Recent studies provide a parallel discovery of tRNA binding by another IFN-induced protein, schlafen 11, which suppresses protein

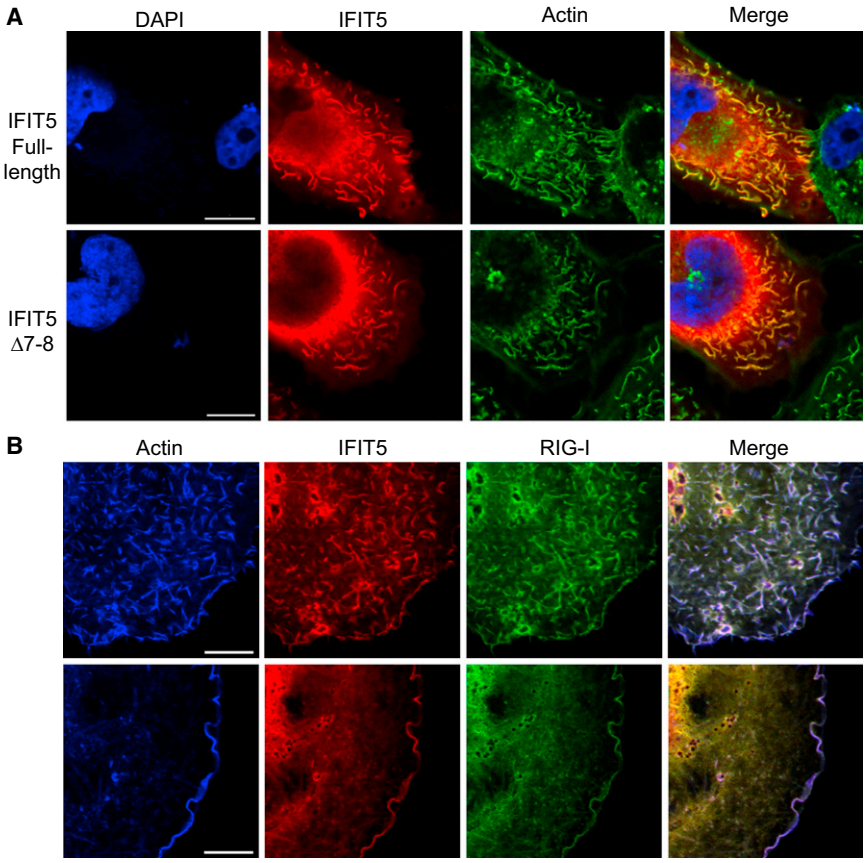


**Figure 4. IFIT5 Localization to Cell-Surface Actin Structures**

Confocal microscopy was performed on fixed cells, focusing on the apical cell surface. Scale bars represent 10 μm.

(A) Fibroblast-derived WI-38 VA-13 cells were transfected to express 3xF-IFIT5 full-length (top panels) or a C-terminal truncation (bottom panels) and imaged for FLAG-tagged protein by indirect immunofluorescence (red). Cells were costained to detect filamentous actin (green) and DNA (blue).

(B) Hepatocyte-derived Huh7 cells were transfected to express mCherry-IFIT5 (red) and eGFP-RIG-I (green). Cells were costained to detect filamentous actin (blue). Different levels of focus show the apical cell surface (top panels) and cell edge (bottom panels) of separate cells.

See also Figure S10.

synthesis by human immunodeficiency virus 1 in a codon-usage dependent manner (van Weringh et al., 2011; Li et al., 2012). In addition to 5′-monophosphate-capped RNAs, IFIT5 also binds RNAs with a 5′ polyphosphate group and thus could have viral as well as cellular RNA ligands. To increase the cellular specificity of RNA interactions, we propose that IFIT5 is regulated by its localization to dynamic actin structures at the cell surface. The membrane-adjacent compartmentalization of IFIT5 and its tRNA binding activity suggest that IFIT5 could impose a localized translational inhibition. Overall, our results expand the eukaryotic repertoire of protein folds for RNA binding, establish a long-sought activity for human IFIT5, define the structural principles by which IFIT5 gained unique function, and introduce another player in the increasingly complex cellular regulation of tRNA.

## EXPERIMENTAL PROCEDURES

Cleared whole-cell extracts were adjusted to 0.2 M NaCl before affinity purification with M2 FLAG antibody resin (Sigma) and elution with triple-FLAG peptide (Sigma). In vivo crosslinking and purification under denaturing conditions were performed as described (Hogg and Collins, 2007b), with controls to ensure no background of RNA binding without crosslinking. N-terminal six-histidine tagged IFIT5 and IFIT1 were expressed in *E. coli* and purified with nickel-charged resin. The iMet tRNA for direct binding assays was transcribed by T7 RNA polymerase with a hammerhead ribozyme to produce the mature tRNA 5′ end (Fechter et al., 1998), gel purified, and radiolabeled with a 5′ monophosphate with T4 polynucleotide kinase. For interrogation of IFIT5-bound RNA 5′ ends, RNA was pretreated with or without 5′ polyphosphatase (Epicentre) and digested with Terminator 5′-monophosphate-dependent exonuclease (Epicentre).

IFIT5 was crystallized by vapor diffusion from 100 mM BisTris (pH 6.5) and 4% (w/v) PEG monomethyl ether 5K. The structure was determined from X-ray diffraction data with multiwavelength anomalous dispersion of selenomethionine-labeled protein crystals. Additional details of the bacterial expression constructs, purifications, crystallization, and structure determination are provided in the Supplemental Experimental Procedures. For microscopy, cells were fixed with 3.7% paraformaldehyde for 10 min, permeabilized with 0.1% Triton X-100 for 15 min, and processed as described (Wong et al., 2002). Actin was visualized with phalloidin conjugated to AlexaFluor 647 or 546 (Invitrogen).

## ACCESSION NUMBERS

Coordinates and structure factors for the IFIT5 crystal structure were deposited in the Protein Data Bank under ID number 3ZGQ.

## SUPPLEMENTAL INFORMATION

Supplemental Information includes Supplemental Experimental Procedures and ten figures and can be found with this article online at http://dx.doi.org/10.1016/j.molcel.2012.12.015.

## ACKNOWLEDGMENTS

We thank members of the Alber, Collins, Shastri, Tjian, Vance, and Welch labs for generously providing reagents, advice, and discussion. We are grateful to James Holton, George Meigs, and Jane Tanamachi at Beamline 8.3.1 at Lawrence Berkeley National Laboratory for help with X-ray data collection. We thank E. Zhang, B. Glaunsinger, and R. Vance for comments on the manuscript. Funding was from the National Institutes of Health (R01 HL079585 to K.C., P50 GM82250 and P01 AI095208 to T.A., and T32 GM007232 to J.M.V.) and a Canadian Institutes of Health Research postdoctoral fellowship (H.J.L.).

Received: November 21, 2012
Revised: December 19, 2012
Accepted: December 20, 2012
Published: January 10, 2013

## REFERENCES

Berke, I.C., Li, Y., and Modis, Y. (2012). Structural basis of innate immune recognition of viral RNA. Cell. Microbiol. *22*, 1328–1338.

Chhabra, E.S., and Higgs, H.N. (2007). The many faces of actin: matching assembly factors with cellular structures. Nat. Cell Biol. *9*, 1110–1121.

Cusack, S., Yaremchuk, A., and Tukalo, M. (1996). The crystal structure of the ternary complex of *T.thermophilus* seryl-tRNA synthetase with tRNA(Ser) and a seryl-adenylate analogue reveals a conformational switch in the active site. EMBO J. *15*, 2834–2842.

D'Andrea, L.D., and Regan, L. (2003). TPR proteins: the versatile helix. Trends Biochem. Sci. *28*, 655–662.

Daffis, S., Szretter, K.J., Schriewer, J., Li, J., Youn, S., Errett, J., Lin, T.Y., Schneller, S., Zust, R., Dong, H., et al. (2010). 2′-O methylation of the viral mRNA cap evades host restriction by IFIT family members. Nature *468*, 452–456.

Delorme-Axford, E., and Coyne, C.B. (2011). The actin cytoskeleton as a barrier to virus infection of polarized epithelial cells. Viruses *3*, 2462–2477.

Diamond, M.S., and Farzan, M. (2013). The broad-spectrum antiviral functions of IFIT and IFITM proteins. Nat. Rev. Immunol. *13*, 46–57.

Farruggio, D., Chaudhuri, J., Maitra, U., and RajBhandary, U.L. (1996). The A1 x U72 base pair conserved in eukaryotic initiator tRNAs is important specifically for binding to the eukaryotic translation initiation factor eIF2. Mol. Cell. Biol. *16*, 4248–4256.

Fechter, P., Rudinger, J., Giegé, R., and Théobald-Dietrich, A. (1998). Ribozyme processed tRNA transcripts with unfriendly internal promoter for T7 RNA polymerase: production and activity. FEBS Lett. *436*, 99–103.

Fensterl, V., and Sen, G.C. (2011). The ISG56/IFIT1 gene family. J. Interferon Cytokine Res. *31*, 71–78.

Geslain, R., and Pan, T. (2011). tRNA: Vast reservoir of RNA molecules with unexpected regulatory function. Proc. Natl. Acad. Sci. USA *108*, 16489–16490.

Hasler, D., and Meister, G. (2012). An argonaute protein directs nuclear xrn2 function. Mol. Cell *48*, 485–486.

Hogg, J.R., and Collins, K. (2007a). Human Y5 RNA specializes a Ro ribonucleoprotein for 5S ribosomal RNA quality control. Genes Dev. *21*, 3067–3072.

Hogg, J.R., and Collins, K. (2007b). RNA-based affinity purification reveals 7SK RNPs with distinct composition and regulation. RNA *13*, 868–880.

Kolakofsky, D., Kowalinski, E., and Cusack, S. (2012). A structure-based model of RIG-I activation. RNA *18*, 2118–2127.

Lange, K. (2011). Fundamental role of microvilli in the main functions of differentiated cells: Outline of an universal regulating and signaling system at the cell periphery. J. Cell. Physiol. *226*, 896–927.

Li, M., Kao, E., Gao, X., Sandig, H., Limmer, K., Pavon-Eternod, M., Jones, T.E., Landry, S., Pan, T., Weitzman, M.D., and David, M. (2012). Codon-usage-based inhibition of HIV protein synthesis by human schlafen 11. Nature *491*, 125–128.

Mukherjee, A., Morosky, S.A., Shen, L., Weber, C.R., Turner, J.R., Kim, K.S., Wang, T., and Coyne, C.B. (2009). Retinoic acid-induced gene-1 (RIG-I) associates with the actin cytoskeleton via caspase activation and recruitment domain-dependent interactions. J. Biol. Chem. *284*, 6486–6494.

Niranjanakumari, S., Lasda, E., Brazas, R., and Garcia-Blanco, M.A. (2002). Reversible cross-linking combined with immunoprecipitation to study RNA-protein interactions in vivo. Methods *26*, 182–190.

Norbury, C.J. (2010). 3′ Uridylation and the regulation of RNA function in the cytoplasm. Biochem. Soc. Trans. *38*, 1150–1153.

Phizicky, E.M., and Hopper, A.K. (2010). tRNA biology charges to the front. Genes Dev. *24*, 1832–1860.

Pichlmair, A., Lassnig, C., Eberle, C.A., Górna, M.W., Baumann, C.L., Burkard, T.R., Bürckstümmer, T., Stefanovic, A., Krieger, S., Bennett, K.L., et al. (2011). IFIT1 is an antiviral protein that recognizes 5′-triphosphate RNA. Nat. Immunol. *12*, 624–630.

Ryder, S.P., Recht, M.I., and Williamson, J.R. (2008). Quantitative analysis of protein-RNA interactions by gel mobility shift. Methods Mol. Biol. *488*, 99–115.

Schoggins, J.W., and Rice, C.M. (2011). Interferon-stimulated genes and their antiviral effector functions. Curr Opin Virol *1*, 519–525.

Schoggins, J.W., Wilson, S.J., Panis, M., Murphy, M.Y., Jones, C.T., Bieniasz, P., and Rice, C.M. (2011). A diverse range of gene products are effectors of the type I interferon antiviral response. Nature *472*, 481–485.

Sen, G.C., and Fensterl, V. (2012). Crystal structure of IFIT2 (ISG54) predicts functional properties of IFITs. Cell Res. *22*, 1407–1409.

Sobala, A., and Hutvagner, G. (2011). Transfer RNA-derived fragments: origins, processing, and functions. Wiley Interdiscip Rev RNA *2*, 853–862.

Stawowczyk, M., Van Scoy, S., Kumar, K.P., and Reich, N.C. (2011). The interferon stimulated gene 54 promotes apoptosis. J. Biol. Chem. *286*, 7257–7266.

van Weringh, A., Ragonnet-Cronin, M., Pranckeviciene, E., Pavon-Eternod, M., Kleiman, L., and Xia, X. (2011). HIV-1 modulates the tRNA pool to improve translation efficiency. Mol. Biol. Evol. *28*, 1827–1834.

Wong, J.M., Kusdra, L., and Collins, K. (2002). Subnuclear shuttling of human telomerase induced by transformation and DNA damage. Nat. Cell Biol. *4*, 731–736.

Yang, Z., Liang, H., Zhou, Q., Li, Y., Chen, H., Ye, W., Chen, D., Fleming, J., Shu, H., and Liu, Y. (2012). Crystal structure of ISG54 reveals a novel RNA binding structure and potential functional mechanisms. Cell Res. *22*, 1328–1338.

Zeytuni, N., and Zarivach, R. (2012). Structural and functional discussion of the tetra-trico-peptide repeat, a protein interaction module. Structure *20*, 397–405.

Zhu, H., Lee, H.Y., Tong, Y., Hong, B.S., Kim, K.P., Shen, Y., Lim, K.J., Mackenzie, F., Tempel, W., and Park, H.W. (2012). Crystal structures of the tetratricopeptide repeat domains of kinesin light chains: insight into cargo recognition mechanisms. PLoS ONE *7*, e33943.

**Molecular Cell, Volume *49***

# Supplemental Information

# tRNA Binding, Structure, and Localization of the Human Interferon-Induced Protein IFIT5

**George E. Katibah, Ho Jun Lee, John P. Huizar, Jacob M. Vogan, Tom Alber, and Kathleen Collins**

## SUPPLEMENTAL EXPERIMENTAL PROCEDURES

**Human Cells**. Cells were grown under standard conditions (37°C, 5% $CO_2$) in DMEM supplemented with 10% tetracycline-free fetal bovine serum and Primocin (Invivogen). HEK293T cells were transfected using either calcium phosphate or Fugene HD (Promega). Huh7 and HeLa cells were transfected with Lipofectamine 2000 (Invitrogen). The SV40-transformed WI-38 VA13 lung fibroblast cell line was transfected with Fugene HD. Stable HEK293 Flp-In T-Rex cell lines expressing 3xF-IFIT5 were generated according to the manufacturer's instructions (Invitrogen) and maintained in 200 μg/ml hygromycin and 10 μg/ml blasticidin (Invitrogen). Cells were treated with 1,000 U/ml human IFN-β (PBL Interferon Source) overnight. To induce 3xF-IFIT5 expression in HEK293 Flp-In T-Rex cell lines, cells were treated with 1 μg/ml doxycycline (Sigma) for 48 h. IFN-β stimulation was verified by immunoblot for phosphorylated Stat1. For confocal microscopy, cells were grown on poly-D-lysine coated coverslips overnight before transient transfection and then were grown for an additional 48-72 h before fixation. Images were acquired on a Zeiss LSM 710 or LSM 780 (Molecular Imaging Center, UC Berkeley) and processed with Zen (Zeiss GmbH).

**Plasmids**. IFIT5 cDNA (Hogg and Collins, 2007a), RIG-I cDNA (R. Vance, UC Berkeley), and other cDNAs (Harvard DNA Resource CORE) were cloned into pcDNA3.1 (Invitrogen) for expression by transient transfection. For transgene cell line generation, 3xF-IFIT5 was cloned into pcDNA5 FRT/TO (Invitrogen). *E. coli* expression constructs were in pET28a (Novagen) with an N-terminal 6-histidine (6xHis) tag and Tobacco Etch Virus (TEV) protease cleavage site (IFIT1) or an N-terminal 6xHis-3xF tag without (Figure 3) or with (Figures 1 and S4, and crystallography) a TEV protease cleavage site (IFIT5).

**Immunoblots**. For inputs, 5-10 μg of cell lysate protein was resolved by electrophoresis and transferred to nitrocellulose. The primary antibodies used were FLAG M2 monoclonal (Sigma), Y701-phosphorylated Stat1 rabbit polyclonal 58D6 (Cell Signaling), hnRNP U monoclonal 3G6 (Santa Cruz Biotechnology), and tubulin monoclonal (Calbiochem), at the following dilutions: FLAG M2 (1:5000), hnRNP U (1:1,000), p-Stat 1 (1:1,000), and tubulin (1:500). Secondary antibodies (IR700 or IR800, Rockland Immunochemicals) were visualized on a LI-COR Odyssey imager.

**Purification of protein and RNA from cell extracts**. Cells were lysed by freeze-thaw in hypotonic buffer containing 20 mM HEPES, pH 7.3, 2 mM $MgCl_2$, 10% glycerol, 0.2 mM ethylene glycol tetraacetic acid, 1 mM DTT, and protease inhibitors. Cells extracts were supplemented with 0.2 M NaCl, 0.1% IGEPAL CA 630, and 0.1% Triton X-100 (IP buffer) and incubated with anti-FLAG M2 resin at 4°C for 1.5 h. Resin was washed three times for 5 min at room temperature with IP buffer containing 0.2% CHAPS and eluted with FLAG peptide for 45 min at 4°C. RNA was recovered from purifications by extraction with TRIzol (Invitrogen) and visualized by denaturing gel electrophoresis

followed by staining with SYBR Gold (Invitrogen), imaged using a Typhoon Trio (Molecular Devices). Synthetic RNAs were used as gel migration standards. For blot hybridization, RNA was transferred to nylon membranes (Hybond N+, GE) and probed with $^{32}$P 5' end-labeled DNA oligonucleotides. Blots to detect tRNA used probe complementary to the tRNA 5' end unless indicated otherwise.

**Protein expression and purification.** For crystallography, IFIT5 was expressed in BL21(DE3)-Rosetta cells induced with 0.2 mM isopropyl β-D-thiogalactopyranoside (IPTG) and grown overnight at 22°C. Selenomethionine (SeMet)-labeled IFIT5 was expressed as described (Van Duyne et al., 1993). Cells were resuspended in Buffer A containing 20 mM HEPES, pH 7.5, 150 mM NaCl, 5 mM imidazole, 1 mM tris(2-carboxyethyl)phosphine (TCEP), 10% glycerol, with protease inhibitor cocktail (Roche). Cells were lysed by sonication. After centrifugation at 35,000x*g* for 1 h, the cleared lysate was applied to a Ni-charged HiTrap FF column (GE Healthcare), and bound proteins were denatured by washing the column with Buffer A containing 6 M guanidine hydrochloride to remove bound RNA. The protein was refolded on the column by washing with Buffer A. Refolded IFIT5 was eluted in Buffer A with 500 mM imidazole, digested with TEV protease to remove the tag, reloaded onto the HiTrap column to remove the tag and the 6xHis-tagged protease, and the flow-through fractions were further purified by gel filtration on a Superdex 75 column (GE Healthcare) in 20 mM HEPES, pH 7.5, 150 mM NaCl, 1 mM TCEP, 5% glycerol. Peak fractions were concentrated with an Amicon 30K centrifuge filter.

EMSAs in Figure 1 and Supplemental Figure S4 used refolded IFIT5; EMSAs in Figure 3 were performed with proteins expressed in BL21(DE3)-RP grown overnight at 18°C in 0.5 mM IPTG and purified by binding to Ni-NTA agarose (Qiagen) in 20 mM HEPES, pH 7.3, 10% glycerol, 2 mM $MgCl_2$, 1 mM TCEP, 1.5 M NaCl, 20 mM imidazole, and protease inhibitors. IFIT1 was similarly expressed and loaded on a HisTrap FF (GE Healthcare) in 20 mM HEPES, pH 7.3, 10% glycerol, 2 mM $MgCl_2$, 1 mM DTT, 0.5 mM TCEP, 1.5 M NaCl, 50 mM imidazole, and protease inhibitors. IFIT5 and IFIT1 were eluted in binding buffer with 300 mM imidazole and 150 mM NaCl, then buffer exchanged with an Amicon 30K centrifuge filter to remove imidazole. Aliquots of all purified proteins were snap frozen in liquid nitrogen and stored at -80°C.

**EMSA**. RNA was gel-purified after transcription using T7 RNA polymerase or, for the anticodon stem-loop RNA, by chemical synthesis. A triphosphate 5' end was created by T7 RNA polymerase initiation. A monophosphate 5' end was added to self-cleaved or synthetic RNAs by T4 polynucleotide kinase. RNA concentration was determined by absorbance, with purified RNA integrity and concentration verified by denaturing gel electrophoresis and SYBR Gold staining. Prior to use, RNA transcripts were folded by heating to 70 °C for 5 min, freezing on ice, addition of 5 mM $MgCl_2$ and 200 mM NaCl, and slow equilibration to room temperature. Binding for EMSAs was performed in 20 mM Tris-HCl, pH 8.0, 200 mM NaCl, 5 mM $MgCl_2$, 10% glycerol, 2 mM DTT, 0.1 mg/ml BSA, with or without 1 mg/ml heparin, with radiolabeled RNA concentration of 0.1 nM. Binding reactions were incubated at room temperature for 45 min before electrophoresis on 0.5X TBE, 5% glycerol, 3 mM $MgCl_2$, 5% (37.5:1) acrylamide:bis-acrylamide gels at 4°C for 2 h in running buffer with 0.5X TBE and 5 mM $MgCl_2$.

**Crystallization and data collection.** Purified IFIT5 (10 mg/ml) was crystallized by vapor diffusion from 100 mM BisTris, pH 6.5, 4~5% (w/v) PEG monomethyl ether 5K. Crystals were transferred to mother liquor containing 25% (w/v) glycerol and frozen in liquid nitrogen. X-ray diffraction data were collected on the Advanced Light Source Beamline 8.3.1 at 100 K. Data to 2.85-Å resolution were collected from SeMet-labeled crystals at peak and remote wavelengths of 0.97965 and 0.96817

Å, respectively, using an inverse-beam strategy. Data (2.20-Å resolution) for native IFIT5 crystals with the same symmetry were collected at 1.1111 Å. Data were processed using the HKL2000 suite (Otwinowski and Minor, 1997).

**Structure determination, refinement, and analysis.** The structure of IFIT5 was determined using multi-wavelength anomalous dispersion phasing using Phenix AutoSol (Adams et al., 2010). The initial model was built by Phenix Autobuild using the phased map derived from the SeMet data and improved using ARP/wARP (Langer et al., 2008), Coot (Emsley and Cowtan, 2004) and Buccaneer (Cowtan, 2006) using the higher resolution native data set (2.2-Å). Refinement was performed using Phenix Refine (Adams et al., 2010) incorporating Translation/Libration/Screw Motion Determination (Painter and Merritt, 2006) procedures with exclusion of 5% of the reflections to calculate $R_{free}$. The final model was validated using Molprobity (Chen et al., 2010). Sequence conservation was mapped onto the structures using Chimera (Pettersen et al., 2004) based on multiple sequence alignment using ClustalW2 (Larkin et al., 2007). Secondary structures were assigned using Dictionary of Protein Secondary Structure (Kabsch and Sander, 1983) and structural figures were generated using PyMOL (http://www.pymol.org) and Chimera.

**EMSA RNA sequences**.
iMet tRNA 64 nt radiolabeled EMSA probe:
AGCAGAGUGGCGCAGCGGAAGCGUGCUGGGCCCAUAACCCAGAGGUCGAUGGAUCGA
AACCAUC
iMet tRNA full length (52 nt and 25 nt RNAs derive from the 5' end of this sequence):
AGCAGAGUGGCGCAGCGGAAGCGUGCUGGGCCCAUAACCCAGAGGUCGAUGGAUCGA
AACCAUCCUCUGCUACCA
iMet tRNA anticodon stem-loop: CUGGGCCCAUAACCCAG
eMet tRNA full length: GCCCUCUUAGCGCAGUGGGCAGCGCGUCAGUCUCAUAAU
CUGAAGGUCCUGAGUUCGAGCCUCAGAGAGGGCACCA
Val-AAC tRNA full length: GUUUCCGUAGUGUAGUGGUUAUCACGUUCGCCUAAC
ACGCGAAAGGUCCCCGGUUCGAAACCGGGCGGAAACACCA
TER: GGAUACCCGCUUAAUUCAUUCAGAUCUGUAAUAGAACUGUCAUUC
AACCCCAAAAAUCUAGUGC
pBSKS(+): GGGCGAAUUGGAGCUCCACCGCGGUGGCGGCCGCUCUAGAA
CUAGUGGAUCCCCCGGGCUGCAGGAAUUCGAU

**Northern blot probes.**
iMet tRNA 5' end: AGCACGCTTCCGCTGCGCCACTCTGCT
iMet RNA 3' end: TAGCAGAGGATGGTTTCGATCCATC
Lys tRNA: AGTCTGATGCTCTACCGACTGAGCTATCCGGGC
Val-AAC tRNA: GGCGAACGTGATAACCACTACACTACGGAAAC
Gly-GCC tRNA: GCAGGCGAGAATTCTACCACTGAACCACCAATGC
Glu-TTC tRNA: GCGCCGAATCCTAGCCACTAGACCACCAGGG
eMet tRNA: AGACTGACGCGCTGCCCACTGCGCTAAGAGGGC
U1 RNA: GGATAAGCCTCGCCCTGGGAA

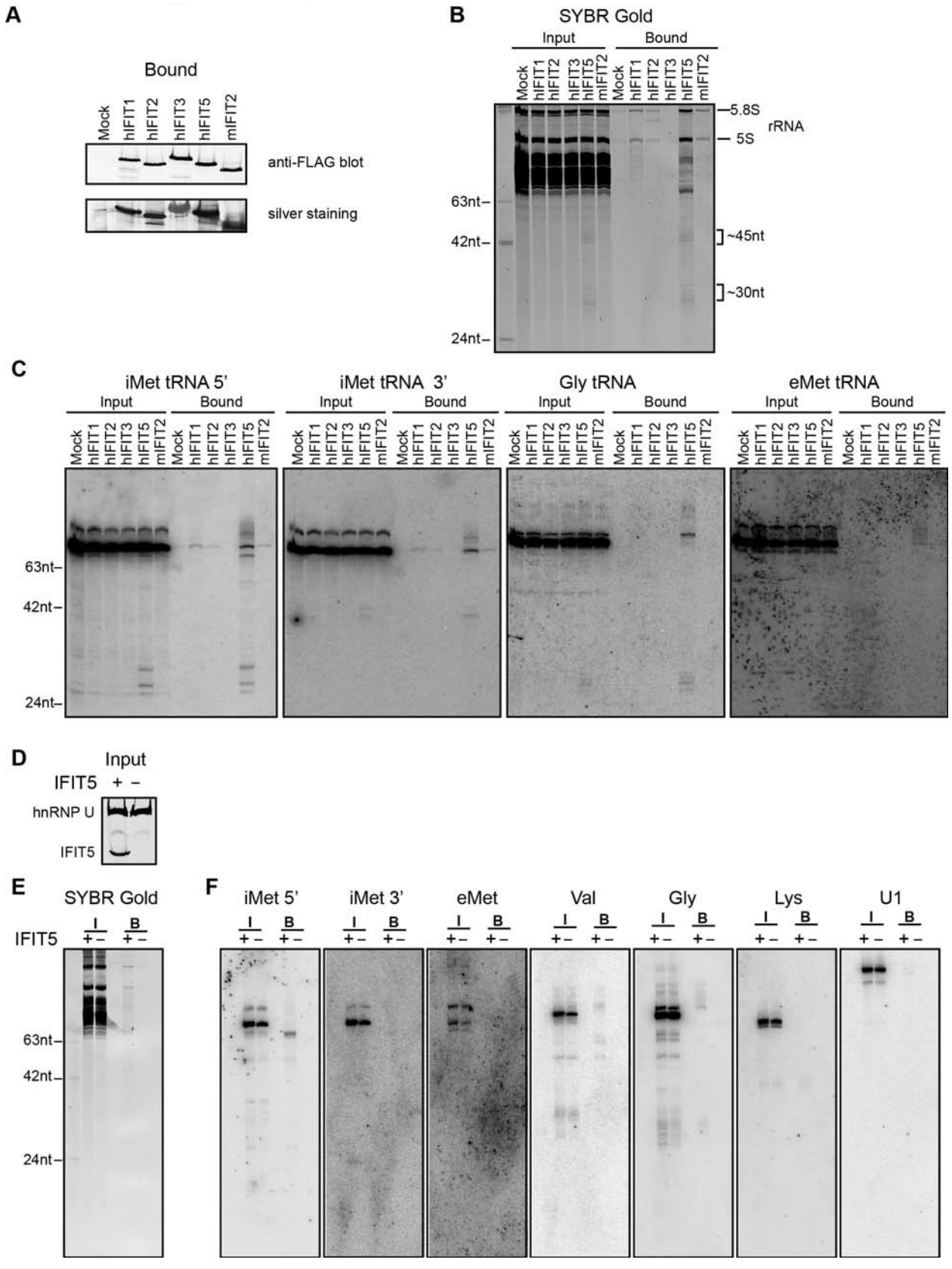
A
Bound
Mock
hIFIT1
hIFIT2
hIFIT3
hIFIT5
mIFIT2
anti-FLAG blot
silver staining
B
SYBR Gold
Input
Bound
5.8S
5S
rRNA
63nt
42nt
24nt
~45nt
~30nt
C
iMet tRNA 5'
iMet tRNA 3'
Gly tRNA
eMet tRNA
D
Input
IFIT5 + –
hnRNP U
IFIT5
E
SYBR Gold
F
iMet 5'
iMet 3'
eMet
Val
Gly
Lys
U1

**Figure S1. IFIT5 association with cellular RNA, Related to Figure 1**

(A-C) IFIT protein co-enrichment of cellular RNA, parallel to the results shown in Figure 1A-C except using cells without IFN-β treatment. HEK293T cells were transfected to express a human IFIT protein or mouse IFIT2, each with an N-terminal 3xF tag. Mock indicates no tagged protein expression. Protein purification was detected by anti-FLAG immunoblot (A, upper panel) or silver staining (A, lower panel), co-purified RNA was resolved by denaturing gel electrophoresis and detected by SYBR Gold staining (B), and blot hybridization of the gel in (B) was used to detect the 5' or 3' end of specific tRNAs (C). IFIT5-dependent ~45 nt and ~30 nt sizes classes of RNA are evident in both input and bound RNA. An irreproducible background of 5.8S and 5S ribosomal RNAs is indicated; this was typically absent with more extensive washing.

(D-F) IFIT5 co-enrichment of RNA demonstrated using transiently transfected HeLa cells. Cells were transfected in parallel to express IFIT5 (+) or empty vector control (-). In (D), hnRNP U provided a normalization control. In (E,F), I indicates input and B indicates bound. U1 is a small nuclear RNA.

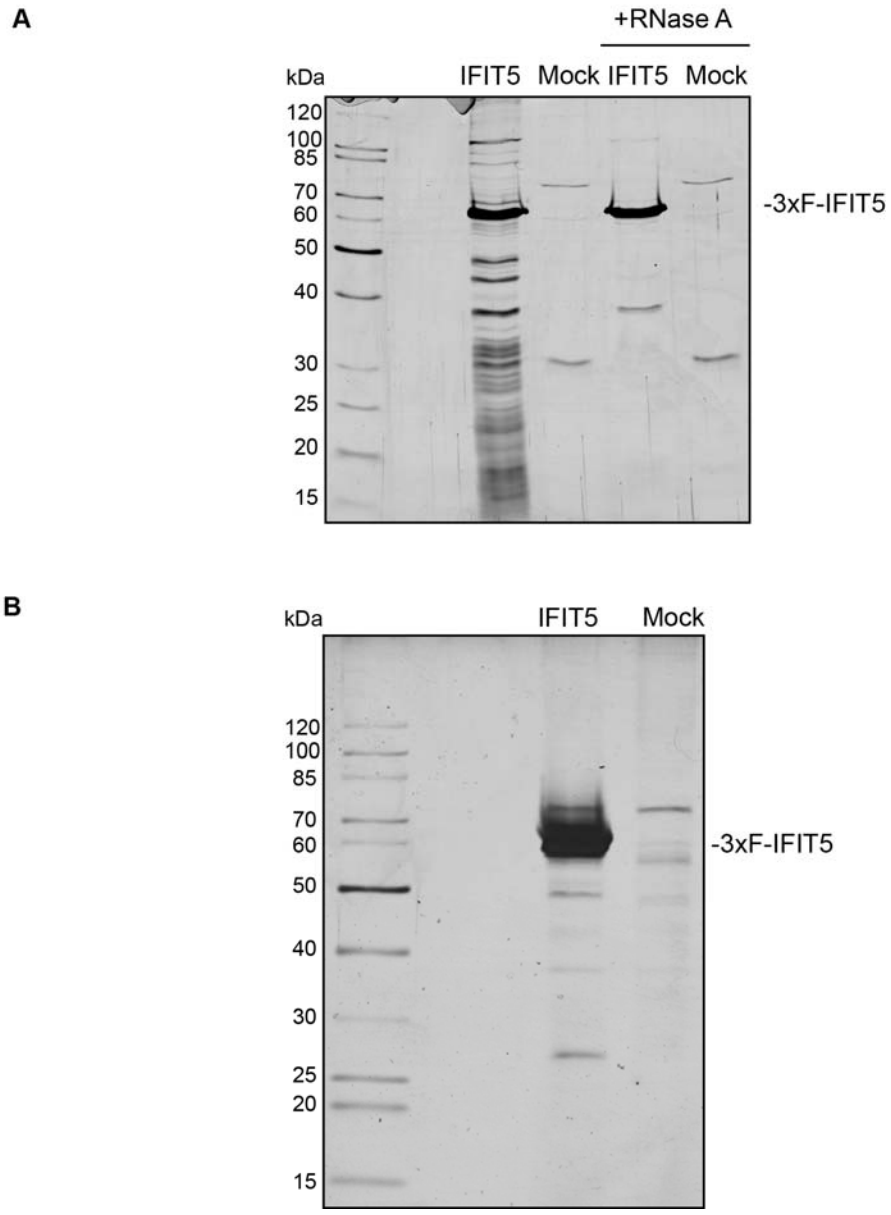


**Figure S2. IFIT5 protein purification, Related to Figure 1**
Silver staining of non-denaturing 3xF-IFIT5 purifications from transiently transfected HEK293T cells (A) or the transgene-integrated HEK293 cell line (B). For RNase treatment, 1 μg/ml RNase A was added during the second wash. Low-abundance proteins smaller than 3xF-IFIT5 could be proteolysis products of the full-length protein.

Mature GTCGATGGATCGAAACCATCCTCTGCTACCA

Sequence 1 GTCGATGGA

Sequence 2 GTCGATGGATCGTAACCA**TTTTTTTTT**

Sequence 3 GTCGATGGATCGAAACCATCCTCTGCTATTTT

Sequence 4 GTCGATGGATCGAAACCATCCTCTGCTATATGGCCGCATATATTT

Sequence 5 GTCGATGGATCTATACCATCCTCTGCTAAAGAAGGGTGCTTTTT

**Figure S3. Sequences of IFIT5-bound iMet tRNA, Related to Figure 1**
Distinct cDNA sequences of iMet tRNA 3' ends obtained by reverse transcription and PCR amplification are listed. Nucleotides in bold (T) or red are genomic mismatches. Potential precursor tRNAs (sequences 3-5) did not appear co-enriched with IFIT5 by blot hybridization, suggesting that they were cloned at relatively high efficiency compared to their purification.

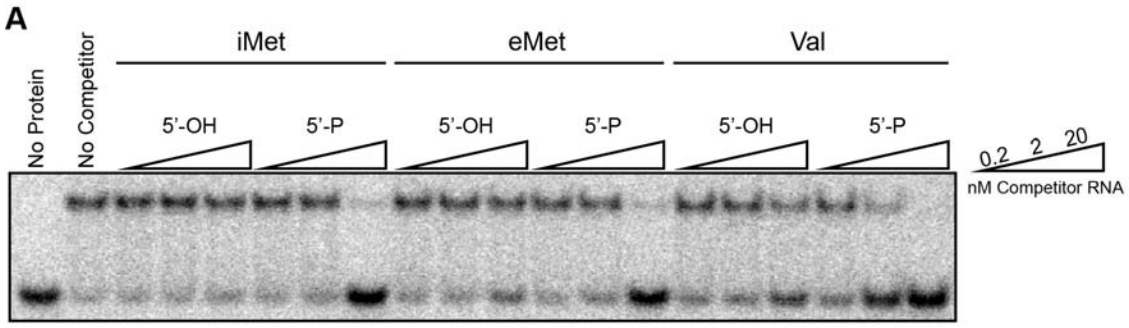
A
No Protein
No Competitor
iMet
eMet
Val
5'-OH
5'-P
5'-OH
5'-P
5'-OH
5'-P
0.2
2
20
nM Competitor RNA

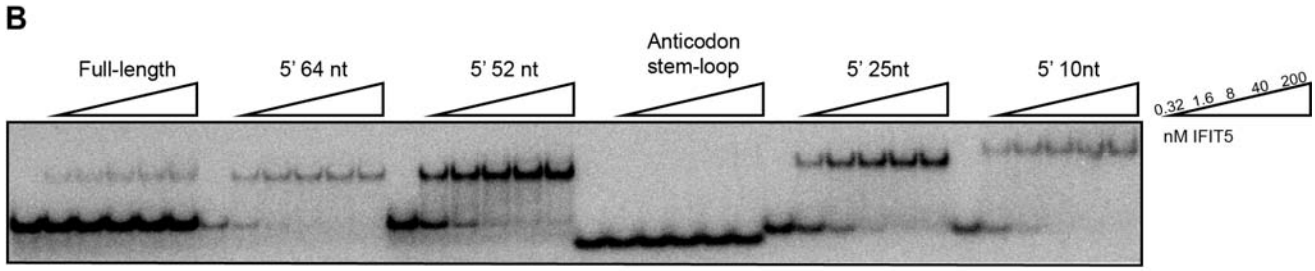
B
Full-length
5' 64 nt
5' 52 nt
Anticodon
stem-loop
5' 25nt
5' 10nt
0.32
1.6
8
40
200
nM IFIT5

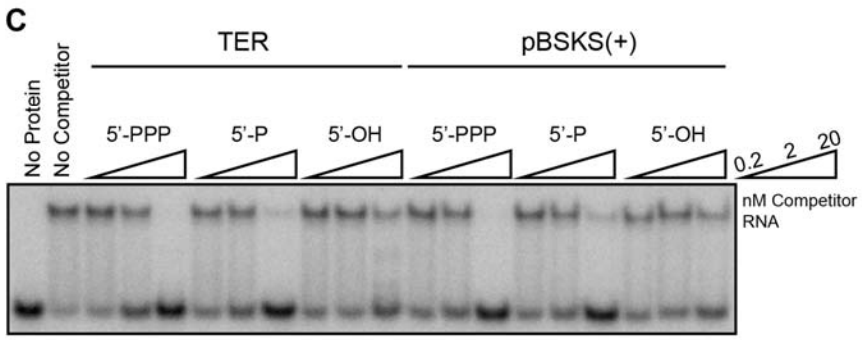
C
No Protein
No Competitor
TER
pBSKS(+)
5'-PPP
5'-P
5'-OH
5'-PPP
5'-P
5'-OH
0.2
2
20
nM Competitor
RNA

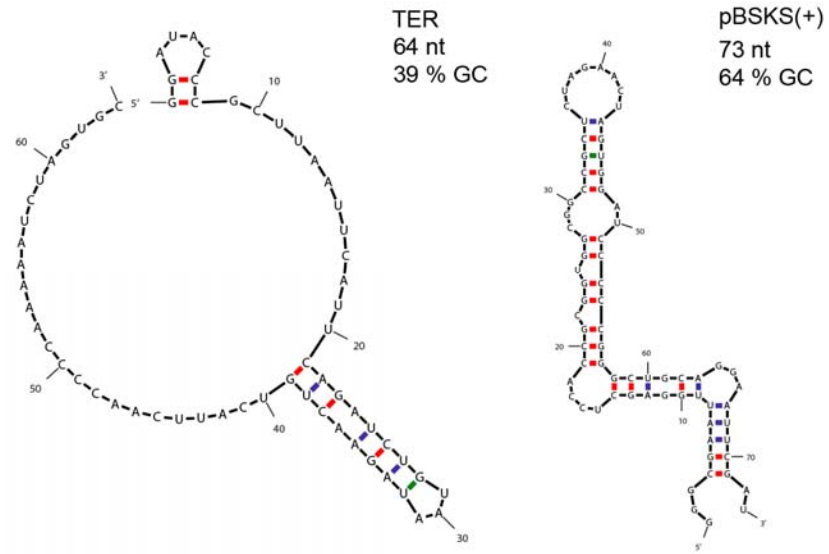
TER
64 nt
39 % GC
pBSKS(+)
73 nt
64 % GC

**Figure S4. In vitro RNA binding specificity of IFIT5, Related to Figure 1**

Unlabeled full-length tRNAs (A) or other RNAs (C) were added to IFIT5 prior to radiolabeled 64-nt iMet tRNA, or different 5'-monophosphate-radiolabeled iMet tRNA regions were tested for IFIT5 binding directly (B). PPP indicates triphosphate, P indicates monophosphate, and OH indicates hydroxyl. TER is a region of *Tetrahymena thermophila* telomerase RNA and pBSKS(+) is a vector polylinker; these sequences are shown with Mfold-predicted secondary structures, lengths, and nt contents.

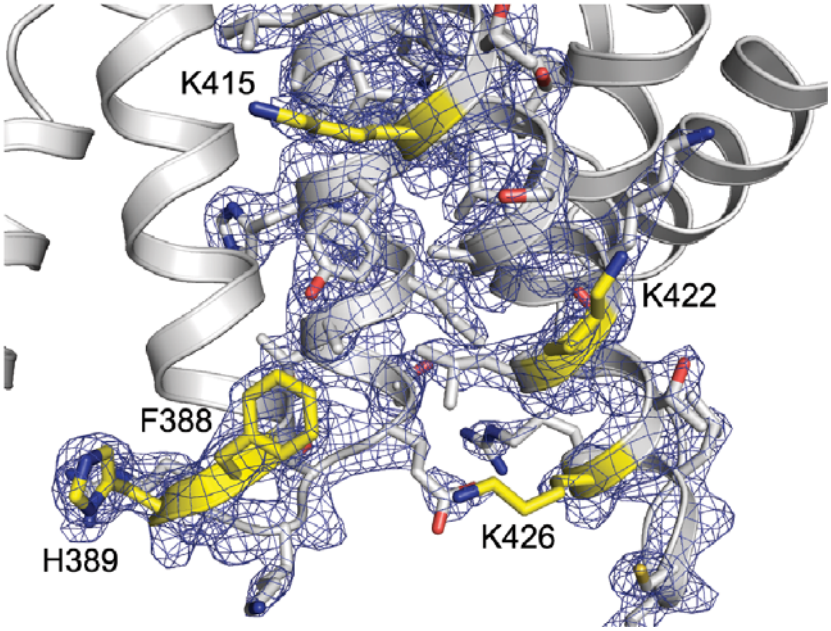


**Figure S5. Representative electron density for IFIT5, Related to Figure 2**
Omit $2F_o$-$F_c$ electron density (1 σ, 2.2-Å resolution) is shown superimposed on the model of TPR7 and the following helix that forms one side of the cleft. Aromatic side chains are clearly visible, and side chains of some of the basic residues including K422 and K426 are disordered.

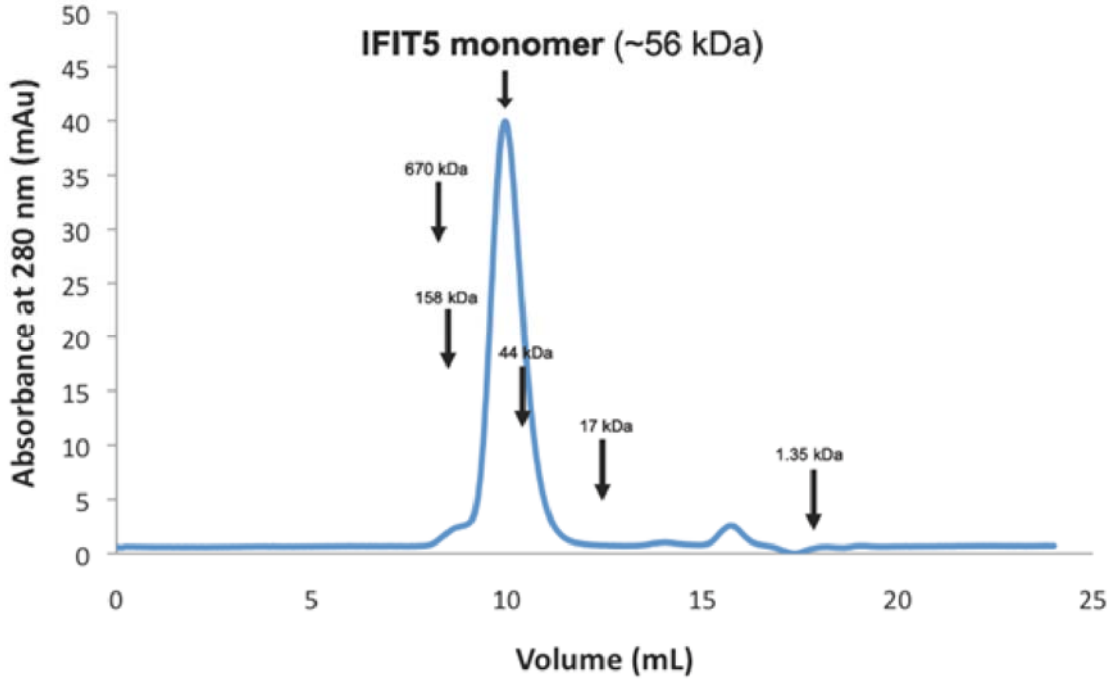


**Figure S6. Gel filtration of the IFIT5 monomer, Related to Figure 2**
A Superdex 75 chromatogram of the purified protein used for crystallography. Elution volumes of the gel filtration standards are indicated with molecular mass (arrows).

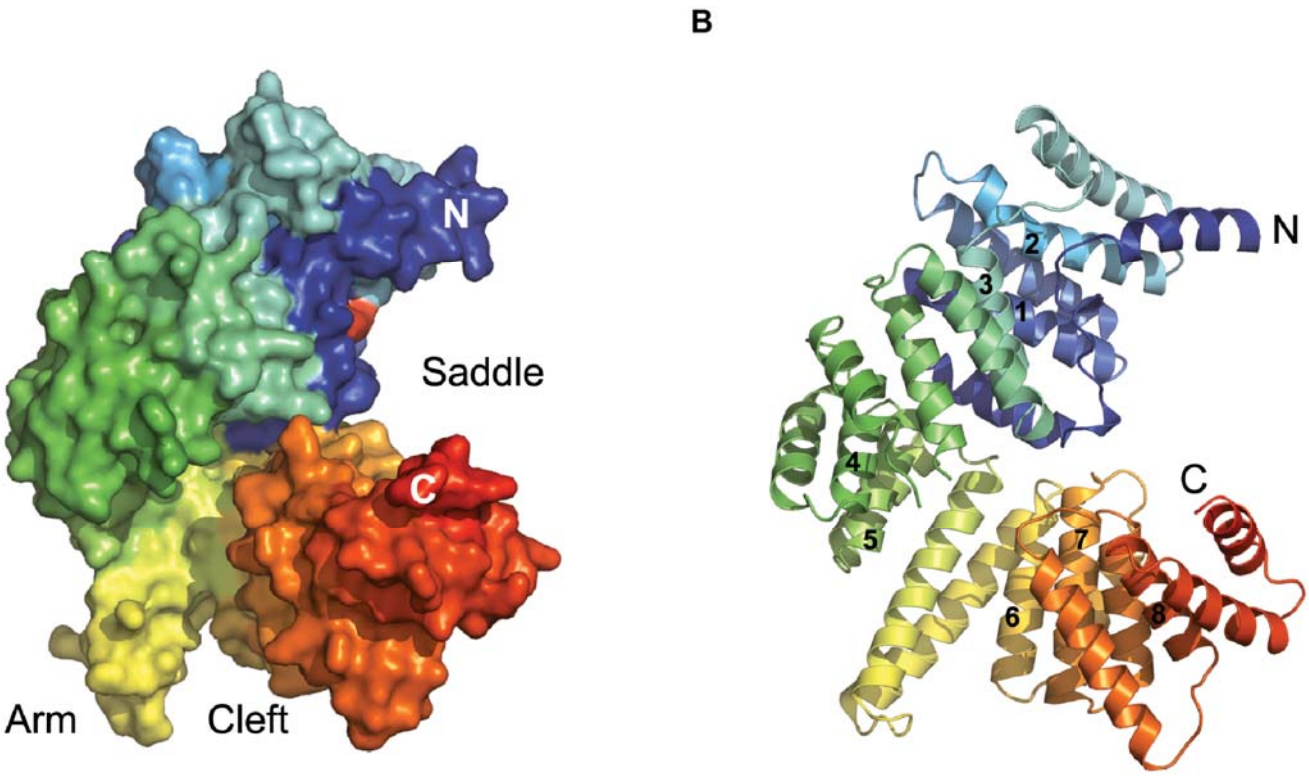


**Figure S7. Path of the chain through the TPR eddy, Related to Figure 2**
Surface representation (A) and ribbon diagram (B) of IFIT5, colored from blue (N-terminus) to red (C-terminus). The protein N- and C-termini are labeled, and the first helices of each TPR are numbered. The N-terminal buttress (dark blue) is followed by TPRs 1-3 (navy blue to dark green) and then a non-TPR helical hairpin and TPRs 4-5 (green to lime). The larger helical hairpin arm (yellow) between TPRs 5 and 6 forms one side of the RNA binding cleft, followed by TPRs 6-8 with two additional helices (orange to red).

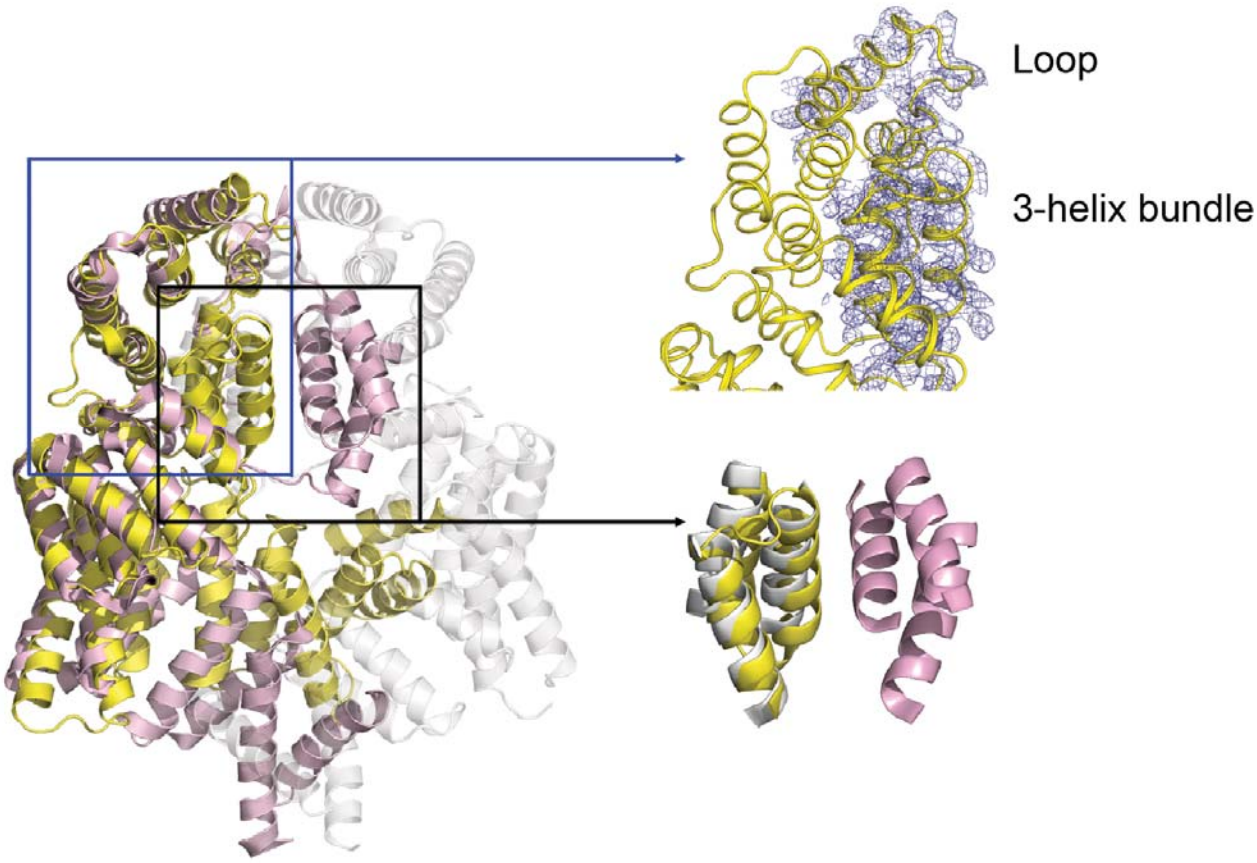


**Figure S8**. **Structural comparison of IFIT5 and IFIT2, Related to Figure 2**
The IFIT5 monomer (yellow) is superimposed on the IFIT2 dimer (individual polypeptides in pink and gray). The unbiased electron density (1 σ, top right) phased with the selenomethionine derivative clearly shows the intramolecular loop connection to the 3-helix bundle within the IFIT5 monomer. In contrast, in the IFIT2 structure, the 3-helix bundle is displaced due to intermolecular domain-swapping (bottom right).


**Figure S9. IFIT protein sequence alignment, Related to Figures 2 and 3**

Sequences are aligned with IFIT5 structural elements, and positions of IFIT5 alanine substitution are indicated with a triangle. HORSE: *Equus caballus*, MACMU: *Macaca mulatta*, CANFA: *Canis familiaris*, BOVIN: *Bos taurus*, CALJA: *Callithrix jacchus*, PONAB: *Pongo abelii*, LOXAF: *Loxodonta africana*, NOMLE: *Nomascus leucogenys*, GORGO: *Gorilla gorilla*, MYOLU: *Myotis lucifugus*, CAVPO: *Cavia porcellus*, OTOGA: *Otolemur garnettii*, SPETR: *Spermophilus tridecemlineatus*, PANTR: *Pan troglodytes*, MACFA: *Macaca fascicularis*, AILME: *Ailuropoda melanoleuca*, MUSPF: *Mustela putorius furo*.

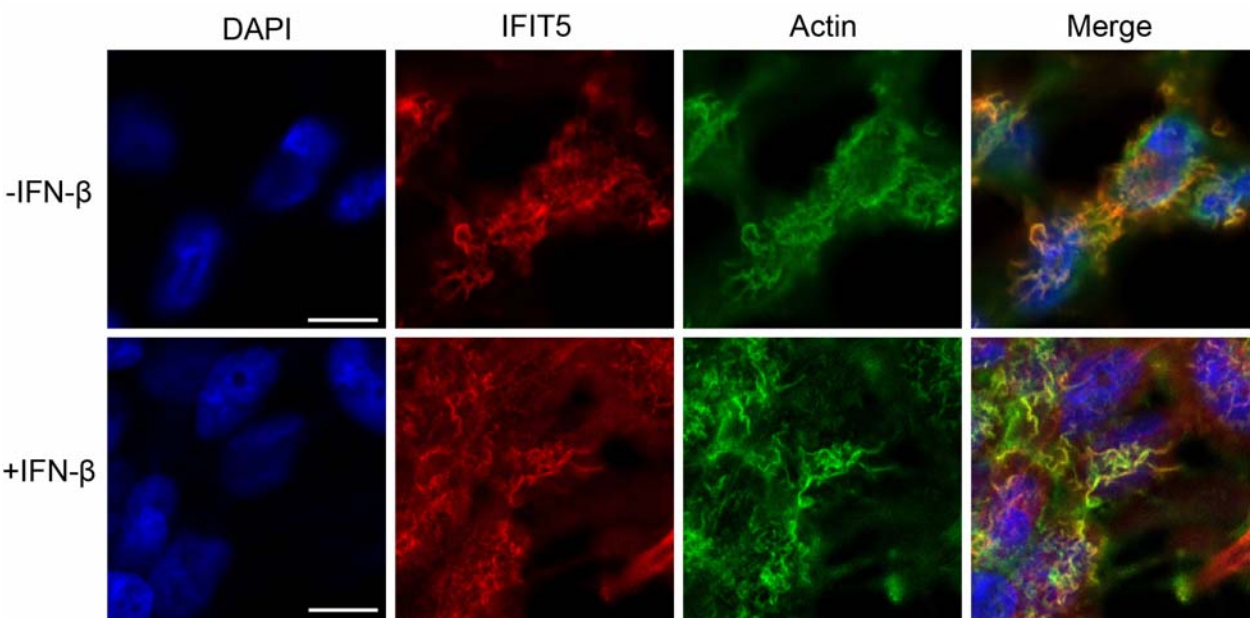


**Figure S10. IFN-independent subcellular localization of IFIT5, Related to Figure 4**
Cells from the transgene-integrated HEK293 cell line with doxycycline-induced expression of 3xF-IFIT5 were imaged for FLAG-tagged protein by indirect immunofluorescence (red). Cells were co-stained to detect filamentous actin (green) and DNA (blue). Scale bars represent 10 microns. Note that HEK 293 cells have less well-spread cytoskeleton than the fibroblast-derived and hepatocyte-derived cells used for the experiments shown in Figure 4.

## SUPPLEMENTAL REFERENCES


Adams, P.D., Afonine, P.V., Bunkoczi, G., Chen, V.B., Davis, I.W., Echols, N., Headd, J.J., Hung, L.W., Kapral, G.J., Grosse-Kunstleve, R.W., et al. (2010). PHENIX: a comprehensive Python-based system for macromolecular structure solution. Acta crystallographica. Section D, Biological crystallography *66*, 213-221.

Chen, V.B., Arendall, W.B., 3rd, Headd, J.J., Keedy, D.A., Immormino, R.M., Kapral, G.J., Murray, L.W., Richardson, J.S., and Richardson, D.C. (2010). MolProbity: all-atom structure validation for macromolecular crystallography. Acta crystallographica. Section D, Biological crystallography *66*, 12-21.

Cowtan, K. (2006). The Buccaneer software for automated model building. 1. Tracing protein chains. Acta crystallographica. Section D, Biological crystallography *62*, 1002-1011.

Emsley, P., and Cowtan, K. (2004). Coot: model-building tools for molecular graphics. Acta crystallographica. Section D, Biological crystallography *60*, 2126-2132.

Hogg, J.R., and Collins, K. (2007). Human Y5 RNA specializes a Ro ribonucleoprotein for 5S ribosomal RNA quality control. Genes Dev. *21*, 3067-3072.

Kabsch, W., and Sander, C. (1983). Dictionary of protein secondary structure: pattern recognition of hydrogen-bonded and geometrical features. Biopolymers *22*, 2577-2637.

Langer, G., Cohen, S.X., Lamzin, V.S., and Perrakis, A. (2008). Automated macromolecular model building for X-ray crystallography using ARP/wARP version 7. Nat. Protoc. *3*, 1171-1179.

Larkin, M.A., Blackshields, G., Brown, N.P., Chenna, R., McGettigan, P.A., McWilliam, H., Valentin, F., Wallace, I.M., Wilm, A., Lopez, R., et al. (2007). Clustal W and Clustal X version 2.0. Bioinformatics *23*, 2947-2948.

Otwinowski, Z., and Minor, W. (1997). Processing of X-ray Diffraction Data Collected in Oscillation Mode. In Macromolecular Crystallography, part A, J. C.W. Carter, and R.M. Sweet, eds. (Academic Press), pp. 307-326.

Painter, J., and Merritt, E.A. (2006). Optimal description of a protein structure in terms of multiple groups undergoing TLS motion. Acta crystallographica. Section D, Biological crystallography *62*, 439-450.

Pettersen, E.F., Goddard, T.D., Huang, C.C., Couch, G.S., Greenblatt, D.M., Meng, E.C., and Ferrin, T.E. (2004). UCSF Chimera--a visualization system for exploratory research and analysis. J. Comput. Chem. *25*, 1605-1612.

Van Duyne, G.D., Standaert, R.F., Karplus, P.A., Schreiber, S.L., and Clardy, J. (1993). Atomic structures of the human immunophilin FKBP-12 complexes with FK506 and rapamycin. J. Mol. Biol. *229*, 105-124.